Smart Mater. Struct. **18** (2009) 055008 (9pp) doi:10.1088/0964-1726/18/5/055008

A nonlinear, control-oriented model for ionic polymer–metal composite actuators

Zheng Chen, Dawn Rochelle Hedgepeth and Xiaobo Tan[1]

Smart Microsystems Laboratory, Department of Electrical and Computer Engineering, Michigan State University, East Lansing, MI 48824, USA

E-mail: chenzhe1@egr.msu.edu, hedgepe1@msu.edu and xbtan@msu.edu

Received 8 December 2008, in final form 23 February 2009
Published 30 March 2009
Online at stacks.iop.org/SMS/18/055008

Abstract

Ionic polymer–metal composites (IPMCs) form an important category of electroactive polymers and have many potential applications in biomedical, robotic and micro/nanomanipulation systems. In this paper, a nonlinear, control-oriented model is proposed for IPMC actuators. A key component in the proposed model is the nonlinear capacitance of the IPMC. A nonlinear partial differential equation (PDE), which can capture the fundamental physics in the IPMC, is fully considered in the derivation of nonlinear capacitance. A systems perspective is taken to get the nonlinear mapping from the voltage to the induced charge by analytically solving the nonlinear PDE at the steady state when a step voltage is applied. The nonlinear capacitance is incorporated into a circuit model, which includes additionally the pseudocapacitance due to the electrochemical adsorption process, the ion diffusion resistance, and the nonlinear DC resistance of the polymer, to capture electrical dynamics of the IPMC. With electromechanical coupling, the curvature output is derived based on the circuit model. The proposed model is formulated in the state space, which will be the starting point for nonlinear controller design. Experimental verification shows that the proposed model can capture the major nonlinearities in the electrical response of the IPMC.

(Some figures in this article are in colour only in the electronic version)

1. Introduction

Electroactive polymers (EAPs) have gained their nickname *artificial muscles* because of their similarity to biological tissues and their built-in actuation capabilities [1]. Ionic polymer–metal composites are one category of ionic EAPs, where the actuation effect arises from electrically induced ion transport. An IPMC sample is made of a thin ion-exchange membrane (e.g. Nafion) sandwiched by two noble metal electrodes, such as platinum or gold [2]. When a small voltage is applied to an IPMC, the movement of hydrated ions leads to redistribution of charge densities inside the IPMC. The resulting electrostatic forces and the accompanying differential swelling are believed to lead to bending [1, 3, 4]. Because IPMCs are soft, resilient, biocompatible, and capable of producing large deformation under a low action voltage, they have many potential applications in biomedical devices [5], biological studies [6], and biomimetic robots [7, 8].

An accurate and practical mathematical model is desirable in the application of IPMCs. Extensive work has been done in modeling of IPMCs. Current modeling work can be classified into three categories based on their complexity levels. Based purely on the empirical responses, *black-box* models, e.g. [9], offer minimal insight into the governing mechanisms within the IPMC. As a more detailed approach, the gray-box models, e.g. [10], are partly based on physical principles while also relying on empirical results to define some of the more complex physical processes. In the most complex form, white-box models with partial differential equations (PDEs), e.g. [3], attempt to explain the underlying physics for the sensing and actuation responses of IPMCs, but they are not practical for real-time control purposes. Del Bufalo *et al* applied mixture theory to the modeling of IPMC actuators [11], but they only addressed the behavior under quasi-static actuation. Chen and co-workers [12, 13] bridged the gap between the empirical models and the physical models for IPMC sensors and actuators, by exactly solving the governing PDEs in the Laplace domain, and coming up with an infinite-dimensional

[1] Author to whom any correspondence should be addressed.

transfer function relating the output to the input. However, this control-oriented model was based on a linear PDE which ignored the nonlinear terms in the physical model. This approximation only holds when a small voltage is applied. A nonlinear model is needed when a relatively high voltage is applied to the IPMC to generate large deformation.

Nonlinear behaviors of IPMCs have been reported in the literature. Chen *et al* [14] employed the Preisach operator to capture the hysteresis in IPMCs. Bonomo *et al* [15] reported a nonlinear circuit model of IPMCs. However, it is an empirical nonlinear model and does not capture the fundamental physics in IPMCs. Nemat-Nasser [4] captured a nonlinear capacitance of IPMCs with an assumption that there is asymmetric charge distribution along the thickness direction and that a cation-depleted layer forms near the anode side when a relatively high voltage is applied. However, the region without cation depletion was still governed by the linear PDE. Porfiri [16] applied Poisson–Nernst–Planck equations to investigate charge dynamics in IPMCs. He used matched asymptotic expansions to solve the nonlinear PDE and obtained a nonlinear circuit model for IPMCs, which includes a nonlinear capacitance and a linear diffusion resistance. However, the circuit model does not accommodate electrochemical reaction near the electrodes and DC resistance of the polymer. No actuation model was further derived based on the circuit model.

Our proposed model is based on the original nonlinear PDE, which can capture ion diffusion, ion migration, and electrostatic interactions in IPMCs. The modeling work starts from the analysis of the equilibrium of IPMCs under a step voltage input, which can be captured by a nonlinear ordinary differential equation (ODE). Numerical analysis of the nonlinear ODE demonstrates an asymmetric charge distribution along the thickness direction. The nonlinear term in the original PDE cannot be ignored when a moderate voltage (>0.2 V) is applied. Since the nonlinear ODE cannot be explicitly solved, a systems perspective is taken to derive the analytical nonlinear mapping from the voltage to the charge. It is verified by the numerical solution, and is practically useful in real-time control.

A nonlinear circuit model is employed to capture the electrical dynamics of IPMCs. It incorporates nonlinear capacitance of IPMCs derived from the nonlinear mapping function between the charge and the voltage, ion diffusion resistance [15, 16], pseudocapacitance due to the electrochemical process at the polymer–metal interface [17], and nonlinear DC resistance of the polymer [15]. Based on the electromechanical coupling effect, the curvature output can be obtained from the electrical dynamic model. The proposed model shows consistency with the linear model when the voltage is small [3]. With definitions of the state variable, input, and output, the model is further presented in the state space, which will be the starting point for nonlinear control design. Parameters are measured or identified through experiments. The proposed model is validated in experiments.

The remainder of the paper is organized as follows. The governing nonlinear PDE is reviewed in section 2. Section 3 shows numerical and analytical procedures for understanding the PDE at the steady state. In section 4, a nonlinear circuit model is introduced to capture the electrical dynamics of IPMCs. The derivation of curvature output of the IPMC and a nonlinear control-oriented model are also shown in section 4. Experimental validation of the proposed model is presented in section 5. Finally, concluding remarks are provided in section 6.

A preliminary version of the paper was presented at the 2008 IEEE Conference on Decision and Control [18].

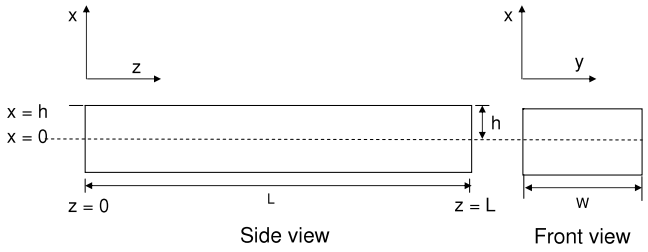

Figure 1. Geometric definitions of an IPMC beam.

2. The governing nonlinear PDE

The governing PDE for charge distribution in an IPMC was first presented in [3] and then used by Farinholt [19] for investigating the actuation and sensing responses. Let **D**, **E**, ϕ, and ρ denote the electric displacement, electric field, electric potential, and charge density, respectively. The following equations hold:

$$\mathbf{E} = \frac{\mathbf{D}}{\kappa_e} = -\nabla\phi, \tag{1}$$

$$\nabla \cdot \mathbf{D} = \rho = F(C^+ - C^-), \tag{2}$$

where κ_e is the effective dielectric constant of the polymer, F is Faraday's constant, and C^+ and C^- are the cation and anion concentrations, respectively. Since the thickness of an IPMC is much smaller than its length or width, we can assume that **D** and **E** are restricted to the thickness direction (x-direction) only, and from here on drop the boldface notation for these variables. Figure 1 shows the geometric definitions of the IPMC.

The continuity expression relates the ion flux J (in the x-direction) to the cation concentration C^+,

$$\frac{\partial J}{\partial x} = -\frac{\partial C^+}{\partial t}. \tag{3}$$

The ion flux consists of diffusion, migration, and convection terms, and can be expressed as [3, 13]

$$J = -\frac{d\kappa_e}{F}\left(\frac{\partial^2 E}{\partial x^2} - \frac{F(1 - C^-\Delta V)}{RT}E\left(\frac{\partial E}{\partial x} + \frac{FC^-}{\kappa_e}\right)\right), \tag{4}$$

where d is the ionic diffusivity, R is the gas constant, T is the absolute temperature, and ΔV is the volumetric change. With the continuity equation (3), one can derive the nonlinear governing PDE in terms of the electric field,

$$\frac{\partial^2 E}{\partial t \partial x} = d\left(\frac{\partial^3 E}{\partial x^3} - \frac{F(1 - C^-\Delta V)}{RT}\left[\frac{\partial^2 E}{\partial x^2}\cdot E + \left(\frac{\partial E}{\partial x}\right)^2\right] - \frac{F^2 C^-(1 - C^-\Delta V)}{RT\kappa_e}\frac{\partial E}{\partial x}\right). \tag{5}$$

In several papers [3, 4, 12, 19], the nonlinear term involving $\frac{\partial E}{\partial x} \cdot E$ in (4) has been ignored based on the assumption

$$\rho(x) = \kappa_e \frac{\partial E}{\partial x} \ll C^- F, \tag{6}$$

resulting in a linear PDE,

$$\frac{\partial \rho}{\partial t} - d\frac{\partial^2 \rho}{\partial x^2} + \frac{F^2 d C^-}{\kappa_e RT}(1 - C^- \Delta V)\rho = 0. \tag{7}$$

However, the assumption (6) will not hold when a relatively high voltage is applied, as to be shown later in this paper.

3. Analysis of the PDE at the steady state

A key component in the proposed model is the capacitance of the IPMC. The first step in our modeling work is to analyze the nonlinear PDE (5) at equilibrium when a step voltage is applied, and find the mapping function from voltage to charge. At equilibrium, $J = 0$. Equation (4) then implies

$$E'' - \frac{(1 - C^- \Delta V)}{FRT} E' \cdot E - \frac{F^2 C^-}{\kappa_e RT}(1 - C^- \Delta V)E = 0, \tag{8}$$

where $E'(x) = \frac{\mathrm{d}E(x)}{\mathrm{d}x}$ and $E''(x) = \frac{\mathrm{d}^2 E(x)}{\mathrm{d}x^2}$. Define

$$a \triangleq \frac{F(1 - C^- \Delta V)}{RT},$$
$$b \triangleq \frac{F^2 C^- (1 - C^- \Delta V)}{RT \kappa_e}.$$

Then (8) becomes

$$E''(x) - aE'(x)E(x) - bE(x) = 0. \tag{9}$$

The following two conditions hold for the ODE.

(1) The overall charge-balance condition leads to

$$\int_{-h}^{h} \rho(x)\,\mathrm{d}x = 0. \tag{10}$$

Since $E'(x) = \frac{\rho(x)}{\kappa_e}$,

$$\frac{1}{\kappa_e}\int_{-h}^{h} \rho(x)\,\mathrm{d}x = E(h) - E(-h) = 0, \tag{11}$$

which implies $E(h) = E(-h)$.

(2) The potential difference is equal to the applied voltage

$$\int_{-h}^{h} E(x)\,\mathrm{d}x = V. \tag{12}$$

Note that $x = -h$ is defined as the anode and $x = h$ is defined as the cathode in this section, so $V \geqslant 0$.

There are two approaches to solving the nonlinear ODE (9), numerical solution and analytical solution. The numerical solution can show the charge distribution, electrical field, and electrical potential along the x direction. The analytical solution can provide a mapping function from the voltage to the charge, leading to the nonlinear capacitance of IPMC. These two approaches will be discussed next.

Table 1. Parameters in the model.

F	R	T	R_i
96 487 C mol^{-1}	8.3143 J mol^{-1} K^{-1}	300 K	18 Ω
R_c	L	W	h
48 Ω	22 mm	10 mm	100 μm
C^-	κ_e	c^{H+}	K_1
1091 mol m^{-3}	1.34×10^{-6} F m^{-1}	1×10^{-6} mol m^{-3}	4×10^5
α_0	Y_e	q_1	
0.129 J C^{-1} [12]	0.56 GPa [12]	210 μC cm^{-2} [20]	
Y_1	Y_2	Y_3	
1×10^{-5} A V^{-1}	1×10^{-4} A V^{-2}	1×10^{-4} A V^{-3}	

3.1. Numerical solution of the PDE at the steady state

In order to numerically solve the second-order ODE (8), one needs to know the boundary conditions $E(-h)$ and $E'(-h)$, or $E(h)$ and $E'(h)$. However, these conditions are unknown. So we change the initial point to $x = x_0$, where x_0 is defined as the zero charge density point, $\rho(x_0) = \kappa_e E'(x_0) = 0$. Note that x_0 will also depend on the applied voltage. In order to satisfy the conditions (11) and (12), we run the following steps recursively.

Step 1: Assign a value to x_0 such that $-h < x_0 < +h$, and a very small value to $E(x_0) = E_0$.

Step 2: Integrate ODE (8) forward from $x = x_0$ to h and backward from $x = x_0$ to $-h$, separately, to get $E(x)$ and $E'(x)$.

Step 3: If $|E(-h) - E(h)| \leqslant \epsilon$, go to step 4; If $E(-h) - E(h) > \epsilon$, decrease $x_0 = x_0 - \epsilon_1$ and go to step 2; if $E(-h) - E(h) < -\epsilon$, increase $x_0 = x_0 + \epsilon_1$ and go to step 2.

Step 4: Do integration $-\int_{-h}^{x} E(x)\,\mathrm{d}x$ to get $\phi(x)$ with $\phi(-h) = 0$.

Step 5: If $|\phi(h) - V| < \epsilon_2$, then go to step 6; if $\phi(h) - V > \epsilon_2$, then increase $E_0 = E_0 + \epsilon_3$ and go to Step 1; if $\phi(h) - V < -\epsilon_2$, then decrease $E_0 = E_0 - \epsilon_3$ and go to step 1.

Step 6: Calculate $\rho(x) = \kappa_e E'(x)$ and do integration $Q = \int_{x_0}^{h} \rho(x) S\,\mathrm{d}x$, then stop.

In the steps above, ϵ, ϵ_1, ϵ_2, and ϵ_2 are small positive constants; $S = WL$ is the surface area of the IPMC. All the physical parameters in the PDE are listed in table 1 and the identification of these parameters is described in section 5. Figure 2 shows the numerical simulation results when $V = 2.61$ V. Figure 2(a) shows the asymmetric charge distribution along the thickness direction. Two inset figures show the details at the turning points of the curve. The negative charge density near the anode approaches the saturation value $C^- F$. The charge density distribution also shows that (6) will not hold in the region close to the boundaries. In other words, the linear PDE will not hold when a high voltage is applied.

Numerical solution offers us insight into the charge distribution, electrical field and electrical potential along the

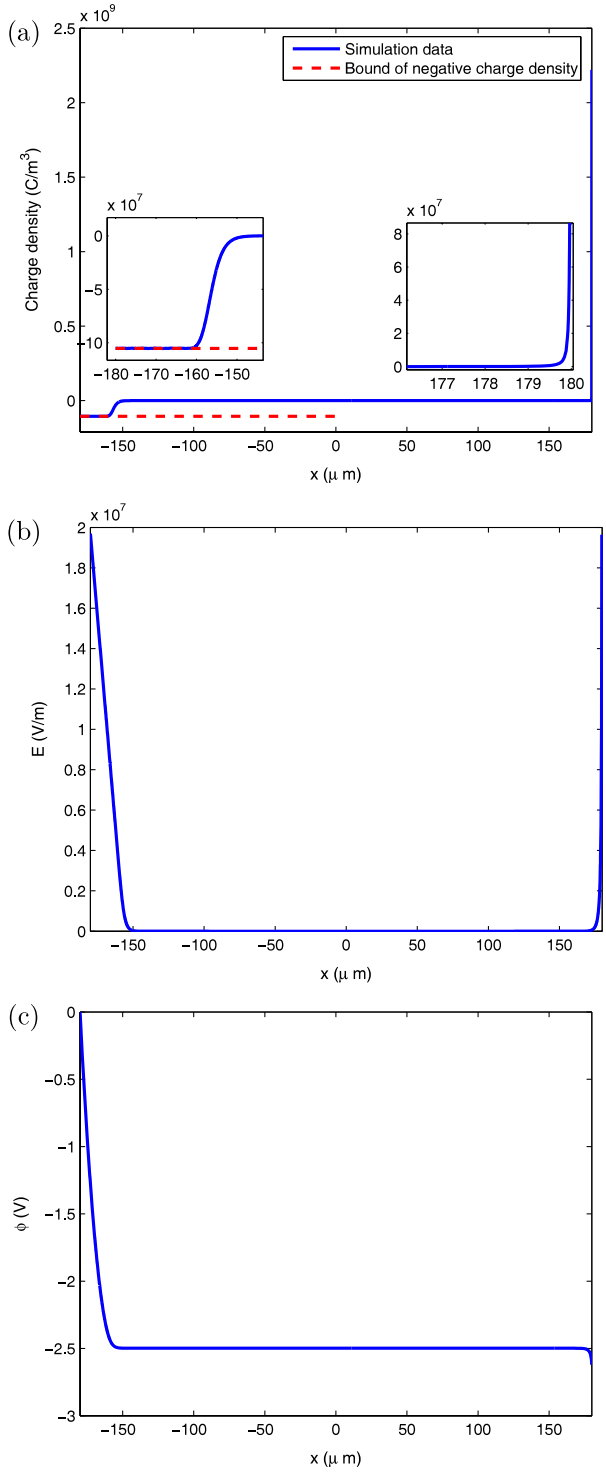

Figure 2. Numerical solution of the nonlinear ODE for $V = 2.61$ V. (a) Charge density; (b) electrical field; (c) electrical potential.

thickness direction for a given step voltage, but it does not provide us an overall picture of the induced charge versus applied voltage. Moreover, the numerical solution takes recursive steps to find proper initial conditions, and requires much computation, which is not practical for control purposes. An analytical solution is practical in real-time implementation. It is also the starting point in the derivation of nonlinear capacitance of IPMC.

3.2. Analytical solution of the PDE at the steady state

Define $y \triangleq E$ and $p \triangleq E'$. Equation (9) becomes

$$\frac{p\,\mathrm{d}p}{(ap+b)} = y\,\mathrm{d}y. \tag{13}$$

We integrate both sides of (13). On the left-hand side we integrate from $p(x_0)$ to p, while on the right-hand side we integrate from $E(x_0)$ to y:

$$\frac{p}{a} - \frac{b}{a^2}\ln\left(\frac{a}{b}p+1\right) = \frac{1}{2}y^2 - \frac{E(x_0)^2}{2}. \tag{14}$$

Let

$$y \triangleq g(p) = \sqrt{2\left(\frac{p}{a} - \frac{b}{a^2}\ln\left(\frac{a}{b}p+1\right)\right) + E(x_0)^2}. \tag{15}$$

Since it is difficult to get an explicit function of $p = g^{-1}(y)$, one cannot continue to solve the ODE equation to get an explicit function $E(x)$. However, we take a systems perspective to solve this problem. What we are really concerned about is how the total charge is analytically related to the input voltage. Then it is not necessary to know the explicit function $E(x)$.

By integrating both sides of (8) from $x = -h$ to h, we get

$$\int_{-h}^{h} E''(x)\,\mathrm{d}x - \int_{-h}^{h} aE'(x)E(x)\,\mathrm{d}x - \int_{-h}^{h} bE(x)\,\mathrm{d}x = 0. \tag{16}$$

With (12), equation (16) can be written as

$$E'(h) - E'(-h) - \frac{a}{2}(E^2(h) - E^2(-h)) - bV = 0. \tag{17}$$

From (11) and (17), one can get

$$V = \frac{1}{b}(E'(h) - E'(-h)). \tag{18}$$

The total charge Q can be obtained by integrating $\rho(x)$ from $x = x_0$ to h, where $\rho(x_0) = 0$:

$$\int_{x_0}^{h} \rho(x)S\,\mathrm{d}x = Q = (E(h) - E(x_0))S\kappa_\mathrm{e}. \tag{19}$$

In section 3.1, figure 2(b) shows that $E(x_0) \ll E(h)$ ($E(x_0) = 1.5 \times 10^{-23}$ V m^{-1} and $E(h) = 2 \times 10^7$ V m^{-1}). So (19) can be written as

$$E(h) = E(-h) = \frac{Q}{S\kappa_\mathrm{e}}. \tag{20}$$

Note that $E'(h)$ and $E'(-h)$ are the positive root and negative root of (14), respectively, when $y = E(h)$.

Define

$$k \triangleq \frac{1}{2}\left(\frac{Q}{S\kappa_\mathrm{e}}\right)^2. \tag{21}$$

Then (14) can be written as

$$\frac{p}{a} - k = \frac{b}{a^2}\ln\left(\frac{a}{b}p+1\right). \tag{22}$$

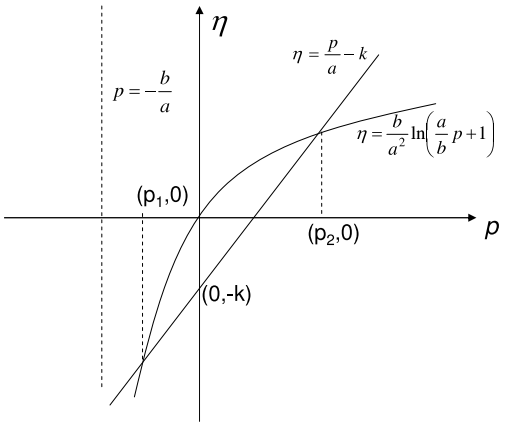

Figure 3. Illustration of solving for p_1 and p_2.

Proposition 3.1. *If* $k > 0$, *there exist two roots* (p_1, p_2) *for (22) such that* $-\frac{b}{a} < p_1 < 0$ *and* $p_2 > 0$. *Furthermore, if* $k = 0$, *then* $p_1 = p_2 = 0$.

See appendix A for the proof of Proposition 3.1.

In order to get the mapping function from V to Q, we need find out how k is related to the distance of two roots $|p_1 - p_2|$. As shown in figure 3, the roots of (22) are the intersection points (p_1 and p_2) of the following two curves:

$$\eta = \frac{b}{a^2}\ln\left(\frac{a}{b}p + 1\right) = f(p),$$
$$\eta = \frac{p}{a} - k = \lambda(p).$$

From figure 3, the negative root p_1 will never hit the line $p = -\frac{b}{a}$ because $p = -\frac{b}{a}$ is the asymptote of the logarithmic function of $\eta = \ln(\frac{b}{a}p + 1)$. The physical explanation of this is the following. Since the negative ions cannot move and the negative ion density is uniform in the IPMC, $\frac{b}{a\kappa_e} = C^- F$ is the bound of the negative charge density. So $p > -\frac{b}{a}$ implies that a layer of depleted positive charges will not form, although the positive charge density can be very close to zero.

Finally, we can write k in terms of the voltage input V

$$k = \bar{\Gamma}(V) \triangleq \begin{cases} \Gamma(V), & V > 0 \\ 0, & V = 0 \end{cases} \tag{23}$$

where

$$\Gamma(V) \triangleq \frac{b}{a^2}\left(\frac{aV}{e^{aV} - 1} - \ln\left(\frac{aV}{e^{aV} - 1}\right) - 1\right), \tag{24}$$

and Γ is continuous at $V = 0$. See appendix B for the derivation of (23). With (21) and (23), one can get the total charge Q as a function of V:

$$Q = S\kappa_e\sqrt{2\bar{\Gamma}(V)}. \tag{25}$$

Note that the nonlinear mapping function from the input voltage is similar to the one reported in [16], which Porfiri obtained by solving the nonlinear PDE with matched asymptotic expansions.

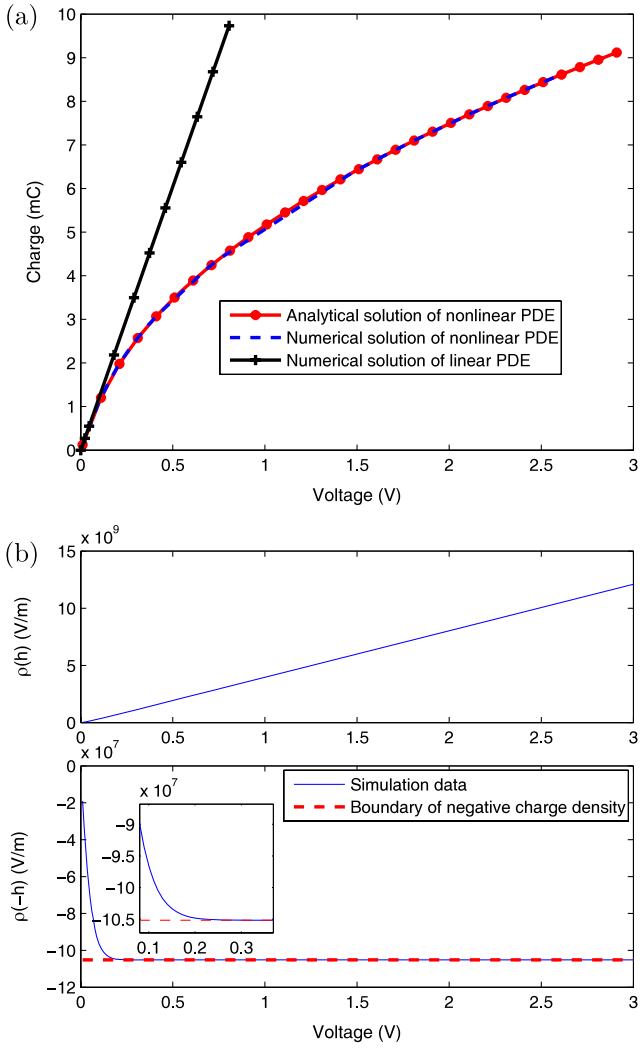

Figure 4. (a) Charge versus voltage at the steady state; (b) charge density at the boundaries versus voltage input.

When $V \to 0$, one can approximate $\bar{\Gamma}(V)$ using its Taylor series expansion around $V = 0$,

$$\bar{\Gamma}(V) \approx \frac{b|V|^2}{8}. \tag{26}$$

Then $Q \approx \frac{\sqrt{b}VS\kappa_e}{2}$, which is consistent with the charge generated in the linear case [3].

Figure 4(a) shows the simulation results of charge versus voltage at the steady state. It includes the results based on the analytical solution of the nonlinear ODE, the numerical solution of the nonlinear ODE, and the numerical solution of the linear ODE (which ignores the nonlinear term), respectively. One can see that the analytical solution matches well the numerical solution of the nonlinear ODE. When the voltage is small, one can ignore the nonlinear term in the nonlinear PDE. However, if a relatively large voltage (>0.2 V) is applied, the error between the nonlinear model and the linear one becomes significant. Figure 4(b) shows the charge densities at the boundaries of the IPMC based on the analytical solution. Note that these densities correspond to the solutions

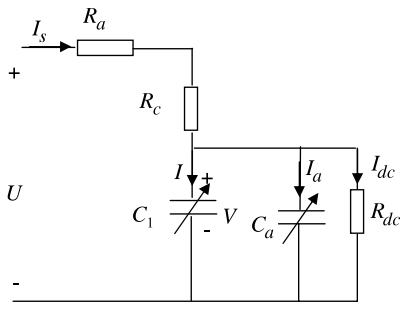

Figure 5. Circuit model of IPMC.

p_1 and p_2 of (22), which can be analytically obtained as shown in appendix B. The figure shows that $\rho(-h)$ cannot go lower than $-C^- F$, but $\rho(h)$ can go arbitrarily high. The inset figure shows the zoom-in view around the turning corner where the negative charge density approaches saturation. It is consistent with the numerical simulation results in figure 2(a). The voltage corresponding to the turning corner is about 0.2 V. The above analytical analysis of PDE at the steady state will be helpful for deriving the nonlinear capacitance of the IPMC, which will be discussed next.

4. Nonlinear circuit model

The above analysis can only capture the nonlinear capacitance of the IPMC. A dynamic model needs to capture the transient processes in the IPMC as well. We propose a nonlinear circuit model, as shown in figure 5. It incorporates the nonlinear capacitance of the IPMC C_1, pseudocapacitance C_a due to the electrochemical adsorption process at the polymer–metal interface, ion diffusion resistance R_c, electrode resistance R_a, and nonlinear DC resistance of the polymer R_{dc}.

4.1. Nonlinear capacitance of the IPMC

The nonlinear capacitance can be obtained by taking the derivative of (25),

$$C_1(V) = \frac{\mathrm{d}Q}{\mathrm{d}V} = S\kappa_e \frac{\Gamma'(V)}{\sqrt{2\Gamma(V)}}, \tag{27}$$

where $\Gamma'(V)$ is the first derivative of $\Gamma(V)$. From (24),

$$\Gamma'(V) = \frac{b}{a}\left(1 - \frac{\mathrm{e}^{aV} - 1}{aV}\right)\frac{\mathrm{e}^{aV} - 1 - aV\mathrm{e}^{aV}}{(\mathrm{e}^{aV} - 1)^2}. \tag{28}$$

The proposed analytical solution of nonlinear capacitance captures the fundamental physics in the IPMC. It is represented by a function in terms of physical parameters and dimensions, and is geometrically scalable.

4.2. Pseudocapacitance due to adsorption

For an electrochemical surface process, e.g. the so-called underpotential deposition of H [20], the following holds:

$$\mathrm{M} + \mathrm{H_3O^+} + \mathrm{e} \overset{K}{\rightleftharpoons} \mathrm{MH_{ads}} + \mathrm{H_2O}, \tag{29}$$

where M is the substrate (usually a noble metal, Pt, Rh, Ru, or Ir). Since IPMC has Pt as electrode and some electrolyte in the polymer, the underpotential deposition process should be incorporated into the model [17]. The adsorption current due to this electrochemical process can be represented by [20]

$$I_a = C_a(V_a)\frac{\mathrm{d}V_a}{\mathrm{d}t}, \tag{30}$$

where

$$C_a(V_a) \triangleq \frac{q_1 SF}{RT}\frac{K_1 c^{\mathrm{H}+}\mathrm{e}^{-\frac{V_a F}{RT}}}{(K_1 c^{\mathrm{H}+} + \mathrm{e}^{-\frac{V_a F}{RT}})^2}. \tag{31}$$

V_a is the voltage on the pseudocapacitance, q_1 is some constant (for H on polycrystalline Pt, $q_1 = 210\ \mu\mathrm{C\ cm^{-2}}$ [20]), $K_1 = \frac{k_1}{k_{-1}}$, k_1 and k_{-1} are the chemical rate constants for forward and reverse directions of (29), and $c^{\mathrm{H}+}$ is the concentration of H^+.

4.3. Nonlinear DC resistance

The current response under a step voltage input will not vanish at the steady state [15] because of the DC resistance of the polymer. One can approximate the DC current by a series of polynomial functions $Y(V)$. In this modeling work, we use a third-order polynomial function:

$$I_{dc} = Y(V) \triangleq \mathrm{sgn}(V)(Y_1|V| + Y_2|V|^2 + Y_3|V|^3). \tag{32}$$

Note that I_{dc} is supposed to be an odd function of V. This is why $\mathrm{sgn}(V)$ appears in (32).

4.4. Curvature output

The induced stress is proportional to the charge density [3]:

$$\sigma = \alpha_0 \rho, \tag{33}$$

where α_0 is the coupling constant. The moment generated by IPMC can be written by

$$M = \int_{-h}^{h} \sigma x W \mathrm{d}x = \int_{-h}^{h} W\alpha_0 x \rho(x)\,\mathrm{d}x. \tag{34}$$

Since $\rho(x) = \kappa_e \frac{\mathrm{d}E}{\mathrm{d}x}$,

$$\begin{aligned} M &= \int_{-h}^{h} W\alpha_0\kappa_e x\,\mathrm{d}E \\ &= W\alpha_0\kappa_e\left(xE|_{-h}^{h} - \int_{-h}^{h} E\,\mathrm{d}x\right). \end{aligned} \tag{35}$$

Since $E(-h) = E(h) = \frac{Q}{S\kappa_e}$, with (25) and $\int_{-h}^{+h} E\,\mathrm{d}x = V$, (35) can be written as

$$M = W\alpha_0\kappa_e(\mathrm{sgn}(V)2h\sqrt{2\bar{\Gamma}(|V|)} - V). \tag{36}$$

If one takes $V \to 0$,

$$M \to W\alpha_0\kappa_e V(h\sqrt{b} - 1) \approx W\alpha_0\kappa_e V h\sqrt{b}, \tag{37}$$

which is consistent with the moment reported in the linear case [3]. One can then obtain the curvature output via

$$\kappa = \frac{M}{Y_e I}, \tag{38}$$

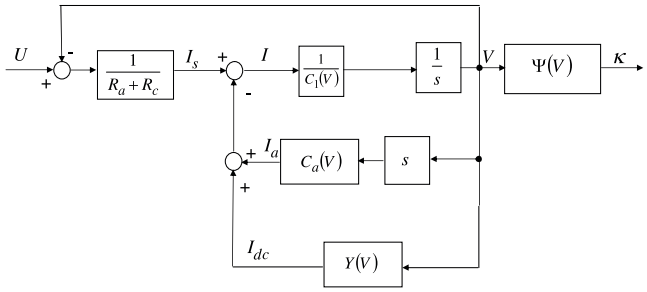

Figure 6. Model structure.

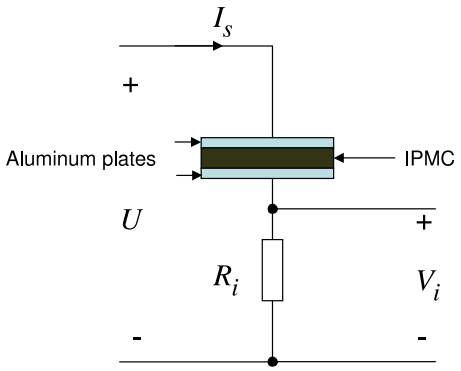

Figure 7. Illustration of experimental set-up.

where $I = \frac{2}{3}Wh^3$ is the moment inertia and Y_e is the equivalent Young's modulus of the IPMC. With (36), equation (38) can be written as

$$\kappa = \Psi(V) \triangleq \frac{3\alpha_0\kappa_e(\mathrm{sgn}(V)2h\sqrt{2\Gamma(|V|)} - V)}{2Y_e h^3}. \tag{39}$$

We note that one could also use nonlinear elasticity theory to model the mechanical output under large deformation [21]. This is outside of the scope of the current paper.

4.5. Nonlinear control-oriented model

The objective of this work is to derive a control-oriented nonlinear model which can be used in controller design. Based on the circuit model (figure 5) and the curvature output (36), the model structure is shown in figure 6.

From (30) and (32), one can get

$$\frac{\mathrm{d}V}{\mathrm{d}t} = \frac{\frac{U-V}{R_a+R_c} - Y(V)}{C_1(V) + C_a(V)}. \tag{40}$$

Defining the state variable $x = V$, the control input $u = U$, and the system output $y = \kappa$, one can obtain a first-order nonlinear dynamic model in the state space:

$$\dot{x} = -\frac{x + Y(x)(R_a + R_c) - u}{(C_1(x) + C_a(x))(R_a + R_c)}, \qquad y = \Psi(x). \tag{41}$$

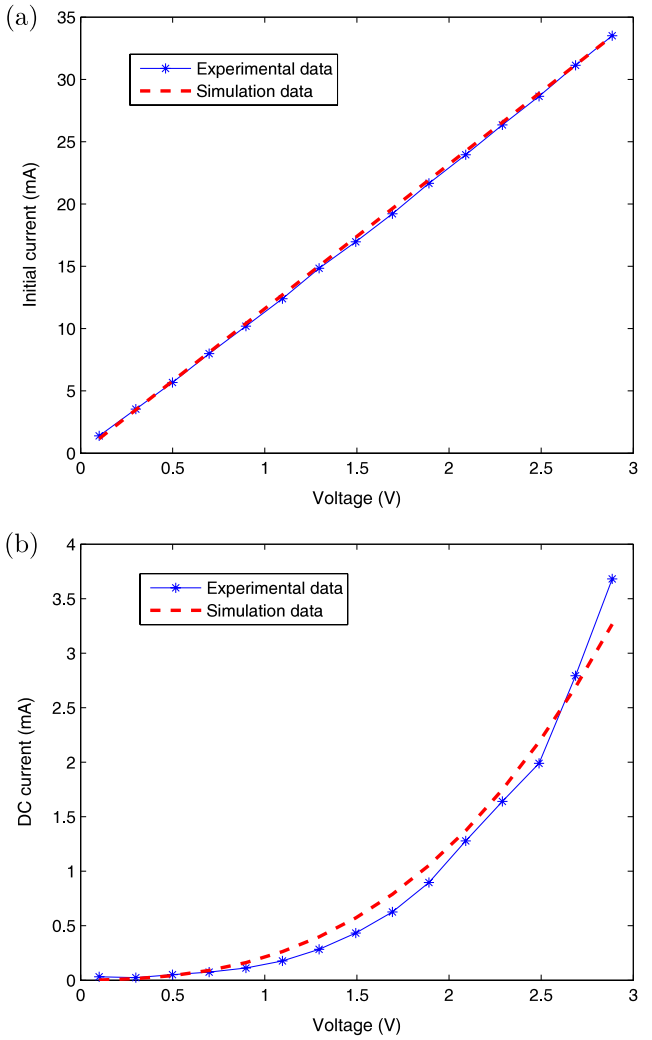

Figure 8. (a) Initial current versus step voltage input; (b) DC current versus step voltage input.

5. Experimental verification

Some physical parameters can be directly measured through the experiments, such as the temperature T, the dimensions L, W, h, the equivalent Young's modulus of the IPMC Y_e, and the electrode resistance R_a. Some parameters are physical constants, such as R, F, q_1. Other parameters $(Y_1, Y_2, Y_3, R_c, K_1, C^-, \kappa_e, \alpha_0)$ can be identified by a model fitting process. To ignore the distributed resistance effect of the electrode on the impedance of the IPMC, we clamped the IPMC sample with two aluminum electrodes, which short circuit the electrode resistance R_a. To measure the current, we added another small resistance $R_i = 18\ \Omega$, which is serially connected with the IPMC. By measuring the voltage V_i, one can obtain $I_s = \frac{V_i}{R_i}$. Figure 7 illustrates the configuration of the experimental set-up. In the rest of this section, R_a is replaced by R_i.

The current responses under a series of step voltage inputs are measured in order to identify these unmeasured parameters. Figure 8 shows the initial current I_{s0} and the DC current $I_{s\infty}$ under step voltage inputs. The initial current I_{s0} is the current

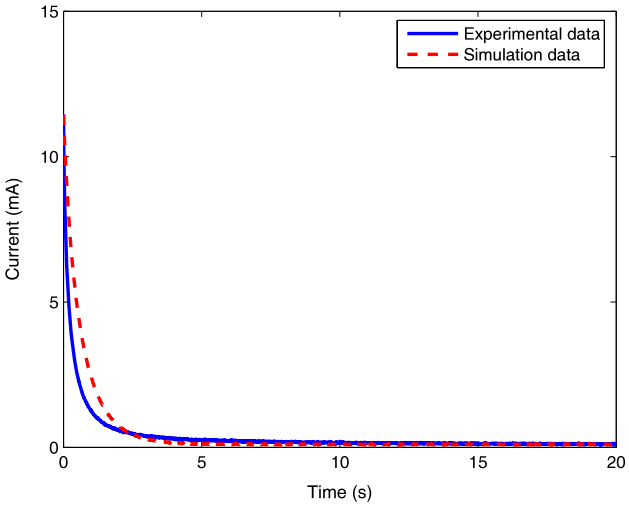

Figure 9. Current response under a step voltage input of 1.0 V.

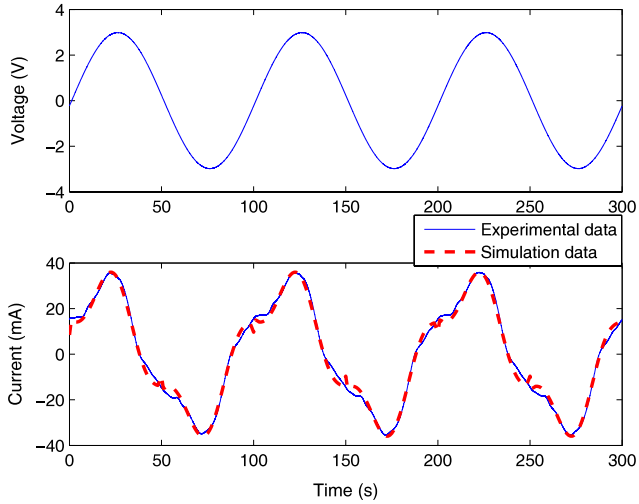

Figure 10. Current response under a sinusoid voltage input.

when the capacitors are uncharged ($V = 0$). The DC current $I_{s\infty}$ is the current when the capacitors have been fully charged. Since the polymer resistance R_{dc} is much larger than R_c, when $V = 0$, one can get (see figure 5)

$$I_{s0} \approx \frac{U}{R_i + R_c}. \tag{42}$$

Figure 8(a) shows that the initial current is a linear function of the step voltage. One can obtain the linear resistance $R_i + R_c$ by calculating the slope of I_{s0} versus U. Figure 8(b) shows that the DC current can be approximated by a third-order polynomial function of V (32), thus the coefficients Y_1, Y_2, Y_3 can be identified. c^{H+}, K_1, κ_e can be tuned to fit the transient process. Figure 9 shows the current responses under a step input of 1.0 V, suggesting that the proposed model can capture both the transient process and the steady state in current responses under a step voltage input. Identification of α_0 was reported in [12]. Table 1 shows all the parameters in the model.

The model is further verified through an experiment to examine the current response under a sinusoid voltage input with frequency 0.01 Hz and amplitude 3 V. Figure 10 shows that the model can predict the current response well.

6. Conclusions and future work

In this work, a nonlinear, control-oriented model is proposed for IPMC actuation. It is derived based on the nonlinear dynamics governing the PDE. Numerical analysis of the nonlinear PDE at the steady state shows an asymmetric charge distribution along the thickness. A systems perspective is taken to obtain a nonlinear mapping from the voltage to the induced charge, which captures the nonlinear capacitance of the IPMC. A nonlinear circuit model is employed to represent the electrical dynamics of the IPMC, including the nonlinear capacitance of the IPMC, the ion diffusion resistance, the pseudocapacitance due to the electrochemical process at the polymer–metal interface, and the nonlinear DC resistance of the polymer. The proposed model is described in the state space, which will be the starting point for nonlinear control design. The proposed nonlinear electrical model is validated experimentally.

The effect of distributed surface resistance is ignored in the presented nonlinear circuit model. In practice, one can consider several segments of the circuit to capture the distributed surface resistance and achieve more precise modeling. However, it will lead to more state variables in the model and more computation in real-time control. This is a tradeoff between model accuracy and implementation complexity.

Future work will be focused on the following: (1) incorporating mechanical dynamics into the model; (2) design of nonlinear controller and nonlinear system analysis; (3) application to IPMC-actuated biomedical devices and biomimetic robots, which require large deformation of the IPMC.

Acknowledgments

This research was supported in part by an NSF CAREER grant (ECCS 0547131), and by MSU IRGP (05-IRGP-418). The authors would like to thank the anonymous reviewers for their useful comments that helped in improving the presentation of this paper.

Appendix A. Proof of proposition 3.1

Proof. Define

$$\chi(p) = \frac{p}{a} - \frac{b}{a^2}\ln\left(\frac{a}{b}p + 1\right) - k, \qquad p > -\frac{b}{a}. \tag{A.1}$$

Let us start with the case when $k > 0$. Because $\chi(0) = -k < 0$, $\chi(p)$ is continuous in $(-\frac{b}{a}, +\infty)$ and

$$\lim_{p\to+\infty} \chi(p) = +\infty > 0, \qquad \lim_{p\to-\frac{b}{a}} \chi(p) = +\infty > 0, \tag{A.2}$$

there exist $p_1 \in (-\frac{b}{a}, 0)$, $p_2 \in (0, +\infty)$ such that $\chi(p_1) = 0$ and $\chi(p_2) = 0$. Since

$$\chi'(p) = \frac{p}{ap + b}, \tag{A.3}$$

with $p > -\frac{b}{a}$, we can get $\chi'(p) > 0$ when $p > 0$ and $\chi'(p) < 0$ when $0 > p > -\frac{b}{a}$. So $\chi(p)$ is monotonically increasing in $(0, +\infty)$, and monotonically decreasing in $(-\frac{b}{a}, 0)$. Then p_1 and p_2 should be unique. When $k = 0$, $\chi(0) = 0$, implying $p_1 = p_2 = 0$. □

Appendix B. Derivation of equation (23)

Define $D \triangleq p_2 - p_1$. Equation (18) can then be written as $V = \frac{D}{b}$. From figure 3,

$$\frac{p_2 - p_1}{\eta_2 - \eta_1} = a, \tag{B.1}$$

where η_1 and η_2 are the η-coordinates corresponding to p_1 and p_2, respectively, in figure 3. Equation (B.1) implies

$$\frac{D}{\frac{b}{a^2}(\ln(\frac{a}{b}p_2 + 1) - \ln(\frac{a}{b}p_1 + 1))} = a. \tag{B.2}$$

With $p_2 = D + p_1$ and (B.2), one can solve p_1 in terms of D,

$$p_1 = \begin{cases} \dfrac{D}{\mathrm{e}^{\frac{a}{b}D} - 1} - \dfrac{b}{a}, & D > 0 \\ 0, & D = 0. \end{cases} \tag{B.3}$$

When $D \to 0$, with l′Hospital′s rule,

$$\lim_{D\to 0}\left(\frac{D}{e^{\frac{a}{b}D} - 1} - \frac{b}{a}\right) = \lim_{D\to 0}\left(\frac{1}{\frac{a}{b}e^{\frac{a}{b}D}}\right) - \frac{b}{a} = 0. \tag{B.4}$$

So p_1 is still a continuous function of D. Since

$$\frac{b}{a^2}\ln\left(\frac{a}{b}p_1 + 1\right) = \frac{p_1}{a} - k, \tag{B.5}$$

from (B.3), one can get

$$\frac{b}{a^2}\ln\left(\frac{a}{b}\left(\frac{D}{e^{\frac{a}{b}D} - 1} - \frac{b}{a}\right) + 1\right) = \frac{1}{a}\left(\frac{D}{e^{\frac{a}{b}D} - 1} - \frac{b}{a}\right) - k. \tag{B.6}$$

Since $D = bV$, one can get equation (23) from equation (B.6). Note that with l'Hospital's rule,

$$\lim_{V\to 0}\left(\frac{aV}{e^{aV} - 1}\right) = \lim_{V\to 0}\left(\frac{a}{ae^{aV}}\right) = 1, \tag{B.7}$$

one gets

$$\lim_{V\to 0}\left(\frac{b}{a^2}\left(\frac{aV}{e^{aV} - 1} - \ln\left(\frac{aV}{e^{aV} - 1}\right) - 1\right)\right) = 0. \tag{B.8}$$

So k is a continuous function of V.

References

[1] Shahinpoor M and Kim K 2001 Ionic polymer–metal composites: I. Fundamentals *Smart Mater. Struct.* **10** 819–33

[2] Kim K J and Shahinpoor M 2003 Ionic polymer–metal composites: II. Manufaturing techniques *Smart Mater. Struct.* **12** 65–79

[3] Nemat-Nasser S and Li J 2000 Electromechanical response of ionic polymer–metal composites *J. Appl. Phys.* **87** 3321–31

[4] Nemat-Nasser S 2002 Micromechanics of actuation of ionic polymer–metal composites *J. Appl. Phys.* **92** 2899–915

[5] Shahinpoor M and Kim K 2005 Ionic polymer–metal composites: IV. Industrial and medical applications *Smart Mater. Struct.* **14** 197–214

[6] Chen Z, Shen Y, Xi N and Tan X 2007 Integrated sensing for ionic polymer–metal composite actuators using PVDF thin films *Smart Mater. Struct.* **16** S262–71

[7] Guo S, Fukuda T and Asaka K 2003 A new type of fish-like underwater microrobot *IEEE/ASME Trans. Mechatron.* **8** 136–41

[8] Tan X, Kim D, Usher N, Laboy D, Jackson J, Kapetanovic A, Rapai J, Sabadus B and Zhou X 2006 An autonomous robotic fish for mobile sensing *Proc. IEEE/RSJ Int. Conf. on Intelligent Robots and Systems (Beijing)* pp 5424–9

[9] Kanno R, Kurata A, Tadokoro S, Takamori T and Oguro K 1994 Characteristics and modeling of ICPF actuator *Proc. Japan–USA Symp. on Flexible Automation* pp 219–25

[10] Newbury K M and Leo D J 2002 Electromechanical modeling and characterization of ionic polymer benders *J. Intell. Mater. Syst. Struct.* **13** 51–60

[11] Del Bufalo G, Placidi L and Porfiri M 2008 A mixture theory framework for modeling the mechanical actuation of ionic polymer metal composites *Smart Mater. Struct.* **10** 1–14

[12] Chen Z and Tan X 2008 A control-oriented and physics-based model for ionic polymer–metal composite actuators *IEEE/ASME Trans. Mechatron.* **13** 519–29

[13] Chen Z, Tan X, Will A and Ziel C 2007 A dynamic model for ionic polymer–metal composite sensors *Smart Mater. Struct.* **16** 1477–88

[14] Chen Z, Tan X and Shahinpoor M 2005 Quasi-static positioning of ionic polymer–metal composite (IPMC) actuators *Proc. IEEE/ASME Int. Conf. on Advanced Intelligent Mechatronics (Monterey, CA)* pp 60–5

[15] Bonomo C, Fortuna L, Giannone P, Graziani S and Strazzeri S 2007 A nonlinear model for ionic polymer metal composites as actuators *Smart Mater. Struct.* **16** 1–12

[16] Porfiri M 2008 Charge dynamics in ionic polymer metal composites *J. Appl. Phys.* **104** 104915

[17] Akle B J 2005 Characterization and modeling of the ionomer–conductor interface in ionic polymer transducers *PhD Thesis* Virginia Polytechnic Institute and State University

[18] Chen Z, Hedgepeth D and Tan X 2008 A nonlinear control-oriented model for ionic polymer–metal composite actuators *Proc. 47th IEEE Conf. on Decision and Control (Cancun)* pp 1851–6

[19] Farinholt K M 2005 Modeling and characterization of ionic polymer transducers for sensing and actuation *PhD Thesis* Virginia Polytechnic Institute and State University

[20] Conway B E 1999 *Electrochemical Supercapacitors Scientific Fundamentals and Technological Applications* (Berlin: Springer)

[21] Fang Y, Pence T J and Tan X 2008 Nonlinear elastic modeling of differential expansion in trilayer conjugated polymer actuators *Smart Mater. Struct.* **17** 065020